Article

Rotaxane-Branched Dendrimers with Enhanced Photosensitization

Wei-Jian Li, Zhubin Hu, Lin Xu, Xu-Qing Wang, Wei Wang, Guang-Qiang Yin, Dan-Yang Zhang, Zhenrong Sun, Xiaopeng Li, Haitao Sun, and Hai-Bo Yang

J. Am. Chem. Soc., **Just Accepted Manuscript** • DOI: 10.1021/jacs.0c07292 • Publication Date (Web): 01 Sep 2020

Rotaxane-Branched Dendrimers with Enhanced Photosensitization

Wei-Jian Li[†], Zhubin Hu[§], Lin Xu[†,*], Xu-Qing Wang[†], Wei Wang[†], Guang-Qiang Yin[†,#], Dan-Yang Zhang[†], Zhenrong Sun[§], Xiaopeng Li[#], Haitao Sun[§,*], Hai-Bo Yang[†,*]

[†]Shanghai Key Laboratory of Green Chemistry and Chemical Processes & Chang-Kung Chuang Institute, School of Chemistry and Molecular Engineering, East China Normal University, 3663 N. Zhongshan Road, Shanghai 200062, P. R. China.

[§]State Key Laboratory of Precision Spectroscopy, School of Physics and Electronic Science, East China Normal University, 500 Dongchuan Road, Shanghai 200241, P. R. China

[#]Department of Chemistry, University of South Florida, Tampa, Florida 33620, United States.

ABSTRACT: During the past few decades, fabrication of functional rotaxane-branched dendrimers has become one of the most attractive yet challenging topics within supramolecular chemistry and materials science. Herein, we present the successful fabrication of a family of new rotaxane-branched dendrimers containing up to twenty-one platinum atoms and forty-two photosensitizer moieties through an efficient and controllable divergent approach. Notably, the photosensitization efficiencies of these rotaxane-branched dendrimers gradually increased with the increase of dendrimer generation. For example, third-generation rotaxane-branched dendrimer **PG3** revealed 13.3-fold higher $^1O_2$ generation efficiency than its corresponding monomer **AN**. The enhanced $^1O_2$ generation efficiency was attributed to the enhancement of intersystem crossing (ISC) through the simple and efficient incorporation of multiple heavy atoms and photosensitizer moieties on the axles and wheels of the rotaxane units, respectively, which has been validated by UV-visible and fluorescence techniques, time-dependent density functional theory calculations, photolysis model reactions, and the apparent activation energy calculations. Therefore, we develop a new promising platform of rotaxane-branched dendrimers for the preparation of effective photosensitizers.

INTRODUCTION

In recent decades, the increasing attention has been paid to the design and synthesis of diverse mechanically interlocked molecules (MIMs) because of their impressive topologies and unique dynamic features,[1] which have enabled them to be versatile platforms for the construction of molecular pumps,[2] molecular elevators,[3] molecular shuttles,[4] and so on.[5] As a vital subset of MIMs, rotaxane-branched dendrimers have become one of the most attractive topics within supramolecular chemistry and materials science.[6] The combination of the characteristics of both rotaxanes and dendrimers endows the resultant rotaxane-branched dendrimers with well-defined topological structures and stimulus-responsiveness.[7] More importantly, the well-defined topological arrangements of rotaxanes within the dendritic skeleton endow the resultant rotaxane-branched dendrimers with amplified collective effects.[8] For instance, we have recently realized a new prototype of rotaxane-branched dendrimers with the collective expansion-contraction motion on each branch for the mimic of the amplified collective molecular motions in biomolecular machines.[9]

Notably, the development of highly effective photosensitizers has recently attracted increasing interests because of their widespread applications in photocatalytic synthetic chemistry and three-dimensional (3-D) printing.[10] According to the photosensitization process and the perturbation theory, the enhancement of the spin-orbit coupling (SOC) can give rise to an increase in the rate constant of the intersystem crossing (k_{ISC}), thereby improving the photosensitization efficiency of photosensitizers.[11] Therefore, the incorporation of heavy atoms such as bromine, iodine, or platinum into a photosensitizer molecule has been one of the most popular approaches for improving the photosensitization efficiency since it can enhance the SOC of photosensitizers.[12] Considering the fact that rotaxane-branched dendrimers usually feature the star-shaped structures and highly branched topology, we envision that rotaxane-branched dendrimers might serve as an advantageous platform for the preparation of the effective photosensitizers for the following reasons: (i) the simple and efficient incorporation of multiple heavy atoms could be realized through the introduction of heavy atoms such as platinum(II) on the axles of the rotaxane units;[13] (ii) the facile substitution of a large number of the photosensitizer moieties on the wheels of rotaxane units may contribute to the enhanced energy transition channels, which should facilitate the ISC process and then improve the photosensitization efficiency;[9b,14] (iii) the spatial steric effect of rotaxane units could reduce the tendency of photosensitizer moieties to aggregate and thereby prevent aggregation-caused quenching (ACQ) effects.[13]

Based on the above considerations as well as our ongoing interests in rotaxane-branched dendrimers,[8,9,13] in this study, a series of new rotaxane-branched dendrimers **PG1**–

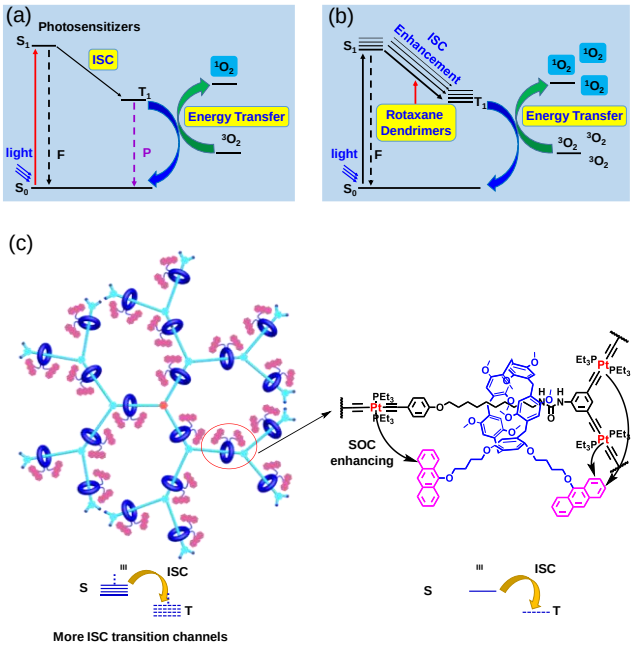

Figure 1. Working mechanism of photosensitizers and the design principle of this work. The different photosensitization processes of the small-molecule photosensitizer (a) and the rotaxane-branched dendrimer photosensitizer (b). (c) Enhanced intersystem crossing of rotaxane-branched dendrimer.

PG3 containing multiple platinum atoms as the heavy atoms and alkoxy-substituted anthracene units as the photosensitizer moieties have been successfully constructed through an efficient and controllable divergent approach. It should be noted that, within the resultant third-generation rotaxane-branched dendrimer **PG3**, twenty-one platinum atoms and forty-two alkoxy-substituted anthracene units were spatially distributed on the axles and wheels of the rotaxane units, thus resulting in the significantly enhanced energy transition channels from S_1 to T_1 and a remarkable heavy-atom effect (Figure 1). As expected, compared with their monomer **AN** and the precursor [2]rotaxane **R-AN**, the newly designed rotaxane-branched dendrimers **PG1–PG3** showed much higher photosensitization efficiency. In particular, the photosensitization efficiencies of these rotaxane-branched dendrimers gradually increased with the increase of dendrimer generation. Accordingly, we demonstrated for the first time that rotaxane-branched dendrimers could serve as a new promising platform for the preparation of effective photosensitizers.

RESULTS AND DISCUSSION

Synthesis and Characterization of Rotaxane-Branched Dendrimers. The key precursor [2]rotaxane **R-AN** containing 9-alkoxy-substituted anthracene was synthesized through multistep sequence reactions as shown in Schemes S1-2. Notably, by employing the threading-followed-by-stoppering approach, the rotaxane formation proceeded in a relatively high yield of 84%. Sequentially, starting from the precursor [2]rotaxane **R-AN**, a controllable divergent strategy was used for the synthesis of the targeted rotaxane-branched dendrimers incorporating mechanically interlocked anthracene-containing units on each branch. As shown in Scheme 1, by employing the copper-catalyzed coupling reaction of the precursor [2]rotaxane **R-AN** with the core module 1,3,5-triethynylbenzene, the first generation of the rotaxane-branched dendrimer **PG1** bearing three rotaxane units with six alkoxy-substituted anthracene moieties on the branches was successfully prepared in a good yield of 74%. The subsequent deprotection of **PG1** with tetrabutylammonium fluoride trihydrate ($Bu_4NF{\cdot}3H_2O$) produced the corresponding rotaxane-branched dendrimer intermediate **PG1-YNE** with six alkyne groups at the periphery. Repeating the similar coupling reaction of **PG1-YNE** and **R-AN** gave rise to the second-generation rotaxane-branched dendrimer **PG2** with nine rotaxane units as well as eighteen alkoxy-substituted anthracene moieties on the branches in 69% yield. Following this iterative deprotection-coupling growth process, the third-generation rotaxane-branched dendrimer **PG3** was obtained in a good yield of 81%. Very impressively, **PG3** contained twenty-one rotaxane units with forty-two alkoxy-substituted anthracene units on the rotaxane branches. Notably, the efficient formation of platinum-acetylide bonds played significant roles in the high-yield and structure-controlled synthesis of the rotaxane-branched dendrimers **PG1–PG3**.[15] Moreover, all of the resultant rotaxane-branched dendrimers were soluble and stable in common organic solvents, which enabled ready purification by means of column chromatography and preparative gel permeation chromatography (GPC).

The rotaxane-branched dendrimers **PG1–PG3** were first characterized by one-dimensional multinuclear (^{1}H and ^{31}P) NMR spectroscopy (Figures S23-24). As shown in the ^{1}H NMR spectra of **PG1–PG3**, the peaks below 0.0 ppm that are assigned to the protons on the axles of the rotaxane units still remained unchanged after the formation of rotaxane-branched dendrimers **PG1–PG3**, which indicated that the rotaxane units remained intact during the synthetic process. From the first to the third generation of the rotaxane-branched dendrimers, these peaks became broader possibly because the rotaxane units on different branches were slightly nonequivalent in the high-generation dendrimers. In the case of ^{31}P NMR analysis, compared with the peak ascribed to the PEt_3 ligands around platinum centers in the precursor [2]rotaxane **R-AN**, those PEt_3 ligands in the rotaxane-branched dendrimers **PG1**, **PG2**, and **PG3** exhibited a remarkable downfield shift of ~2.9 ppm, respectively, which provided a direct evidence for the formation of platinum-acetylide bonds during the dendrimer growth process.

Mass spectrometric investigation of the rotaxane-branched dendrimers **PG1–PG3** was performed by the matrix-assisted laser desorption/ionization time of flight mass spectrometry (MALDI-TOF-MS), which provided the further support for the existence of the desired rotaxane-branched dendrimers. In the MALDI-TOF-MS spectrum of the rotaxane-branched dendrimer **PG1**, the peak of m/z = 7360.3, consistent with the theoretical values of the [**PG1** + H]$^+$ ion (m/z = 7,357.6), was detected (Figure S15). The MALDI-TOF-MS spectrum of the rotaxane-branched

Scheme 1. (a) Synthesis of Rotaxane-Branched Dendrimer PG1. (b) Schematic Representation of A Controllable Divergent Strategy for the Synthesis of Rotaxane-Branched Dendrimers PG2 and PG3. Reaction Conditions: (I) (i) $Bu_4NF{\cdot}3H_2O$, THF, r.t., 2 h; (ii) R-AN, CuI, DCM/Et_2NH, r.t., overnight, 69%; (II) (i) $Bu_4NF{\cdot}3H_2O$, THF, r.t., 2 h; (ii) R-AN, CuI,DCM/Et_2NH,r.t.,overnight, 81%.

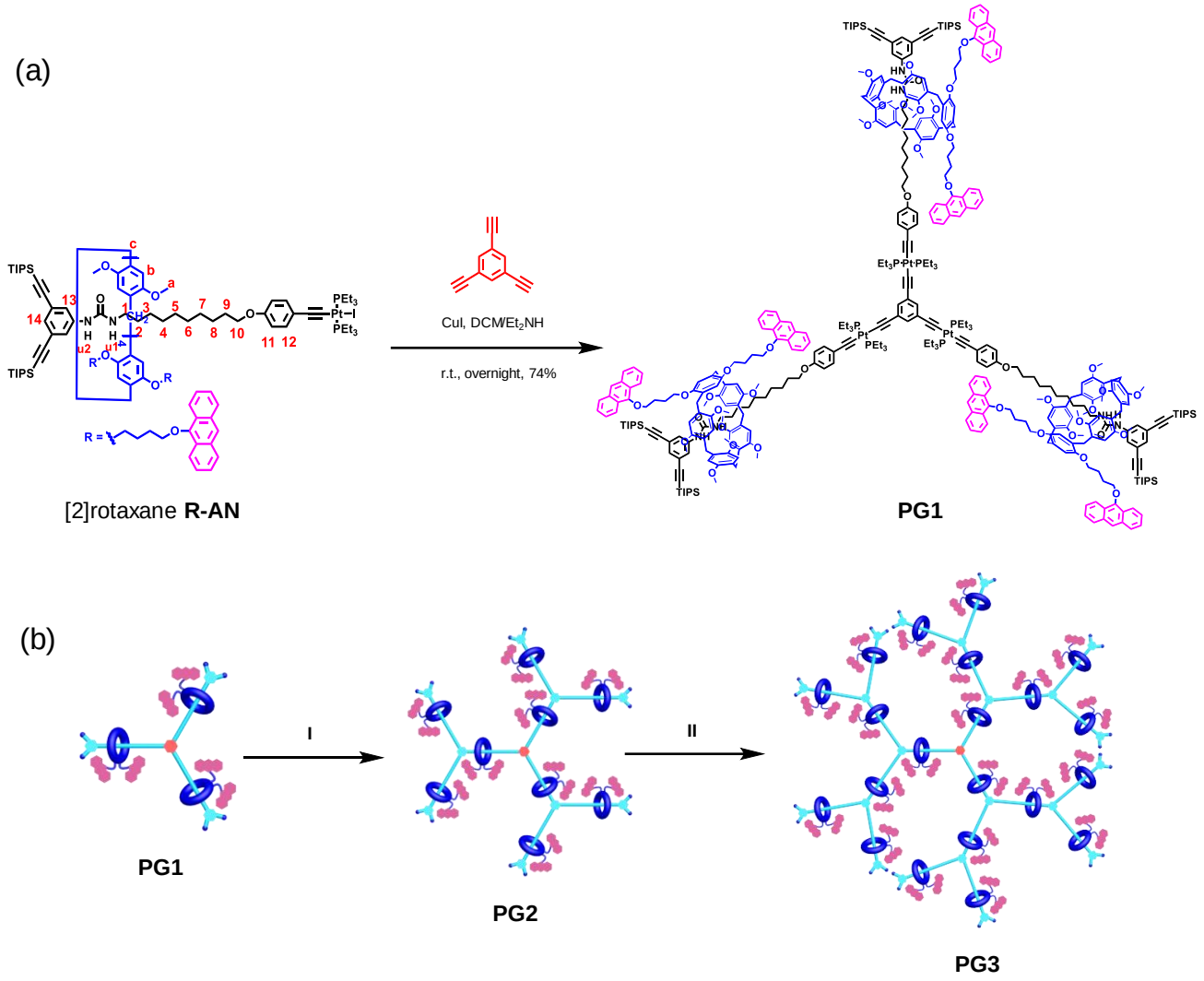

dendrimer **PG2** exhibited two charged states at m/z = 20,856.7 and 10,437.6 corresponding to [**PG2** + K]$^+$ and [**PG2** + K + Na]$^{2+}$, respectively, which were close to their theoretical molecular weights (m/z = 20,854.1 and 10,438.5) (Figure S19). For the rotaxane-branched dendrimer **PG3**, MALDI-TOF-MS provided unsatisfactory mass data because of its high molecular weight (theoretical average M = 47,781.00 Da) and low ionization efficiency. To determine the large, monodispersed rotaxane-branched dendrimers, two-dimensional (2-D) diffusion-ordered spectroscopy (DOSY) was also exploited to evaluate the resultant rotaxane-branched dendrimers **PG1–PG3** (Figures S26-28). The observation of a distinct band in the DOSY spectrum of **PG1**, **PG2**, or **PG3** indicated the existence of the sole species of rotaxane-branched dendrimers. Furthermore, a significant decrease in the diffusion coefficient (D) from $(1.38 \pm 0.12) \times 10^{-9}$ m^2 s^{-1} (**PG1**) to $(1.02 \pm 0.10) \times 10^{-9}$ m^2 s^{-1} (**PG2**), $(6.76 \pm 0.15) \times 10^{-10}$ m^2 s^{-1} (**PG3**) was observed, which provided further evidence of the progressive size increase of the obtained rotaxane-branched dendrimers. Moreover, dynamic light scattering (DLS) investigations of rotaxane-branched dendrimers **PG1–PG3** were also conducted to determine their sizes in solution (Figure S29). The average hydrodynamic sizes (D_h) for **PG1**, **PG2**, and **PG3** were 2.2 ± 0.1 nm, 3.6 ± 0.2 nm, and 6.2 ± 0.2 nm, respectively, which indicated that the size progression was in agreement with that measured by the DOSY technique.

With the aim of identifying the morphologies, atomic force microscopy (AFM) measurements of the resultant rotaxane-branched dendrimers **PG1–PG3** were also carried out as well. As shown in Figure 2, when the generation of the dendrimers increased, the averaged height gradually increased from 2.1 ± 0.1 nm (**PG1**) to 3.4 ± 0.1 nm (**PG2**), and 5.5 ± 0.2 nm (**PG3**), respectively. These results also provided a reasonable evidence for the successful preparation of high-generation rotaxane-branched dendrimers.

Photosensitization Efficiencies of Rotaxane-Branched Dendrimers. After introduction of the anthracene unit as the photosensitizer, we investigated the photosensitizing ability of the resultant rotaxane-branched dendrimers

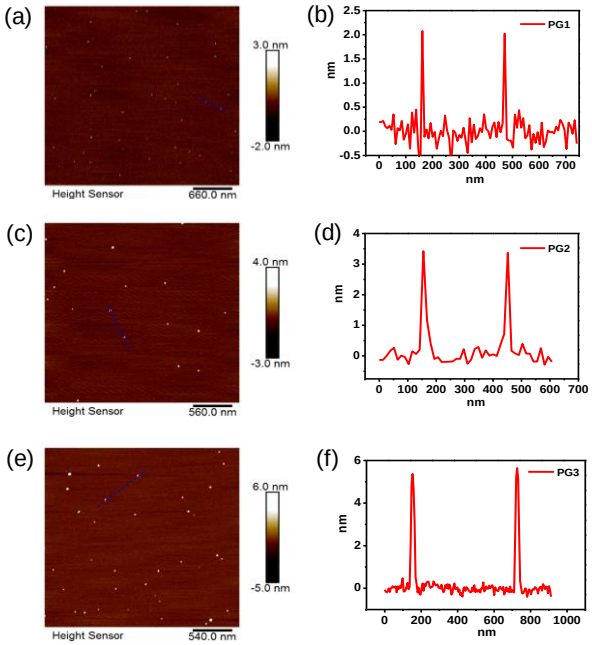

Figure 2. AFM images of the rotaxane-branched dendrimers. (a) **PG1**; (b) the height range of **PG1** is 2.1 ± 0.1 nm; (c) **PG2**; (d) the height range of **PG2** is 3.4 ± 0.1 nm; (e) **PG3**; (f) the height range of **PG3** is 5.5 ± 0.2 nm.

PG1–PG3 as well as the precursor [2]rotaxane **R-AN** and the monomer **AN**. The photophysical data of all compounds are summarized in Table 1. At the equal anthracene unit concentrations (0.042 mM) in THF, all compounds displayed two main absorption peaks at approximately 370 nm and 391 nm with almost the same molar absorption coefficient and had the similar wavelengths of maximum photoluminescence (PL) emission at approximately 420 nm. This observation indicated that the intermolecular or intramolecular interactions between anthracene groups and the aggregation of anthracene moieties did not take place even in the case of **PG3,** which contained forty-two anthracene units (Figures 3a-b). However, as the generation of the dendrimers increased, the fluorescence intensity decreased progressively accompanied by a decreased fluorescence quantum yield (Φ_f) from 35.3 ± 2.6% (**AN**) and 17.1 ± 2.1% (**R-AN**) to 10.8 ± 1.3% (**PG1**), 8.0 ± 1.0% (**PG2**), and then to 6.7 ± 0.8% (**PG3**), which might be attributed to the gradual enhancement of the intersystem crossing (ISC) from **AN** to **PG3** (Figure 3c).

As one of the most important parameters of photosensitizers, the $^1O_2$ generation efficiency (Φ_o) of **PG1–PG3**, **R-AN**, and **AN** was evaluated by using the commercially available $^1O_2$ indicator singlet oxygen sensor green (SOSG), which could react with the generated $^1O_2$ to give green fluorescence with a maximum emission wavelength at 550 nm.[16] Interestingly, as shown in Figure 3d, along with the increase of dendrimer generation from **PG1** to **PG2** and then to **PG3**, the normalized Φ_o increased from 1.0 to 2.5 and then to 7.3. Notably, the third-generation rotaxane-branched dendrimer **PG3** showed approximately 7-fold higher $^1O_2$ generation than that of the first-generation rotaxane-branched dendrimer **PG1**. Although **R-AN** and **AN** also had anthracene moieties, the change in fluorescence intensity of SOSG was negligible under the light irradiation of the mixture solution of SOSG and **R-AN** or **AN** for 60 min, which revealed the very low efficiency of $^1O_2$ generation by **R-AN** and **AN** (Figures S35-36). More importantly, the inverse correlation between Φ_o and Φ_f indicated that increasing the generations of rotaxane-branched dendrimers was an effective way to enhance the ISC in the above-mentioned cases.

Table 1. Optical and photosensitization properties of the resultant rotaxane-branched dendrimers **PG1–PG3**, the precursor [2]rotaxane **R-AN** and the monomer **AN**.

Compound	Φ_f (%)	λ_{abs} (nm)	λ_{em} (nm)	Ak[a]	$^1O_2$ normalized yield
AN	35.3±2.6	370, 391	419	18.1±2.4	0.5[b]
R-AN	17.1±2.1	371, 391	420	21.5±2.2	0.6[b]
PG1	10.8±1.3	370, 391	420	33.3±1.6	1.0
PG2	8.0±1.0	370, 391	420	82.1±5.0	2.5
PG3	6.7±0.8	371, 391	420	241.5±4.2	7.3

[a] The non-linear regression fitting parameters of the $^1O_2$ generation rate equation. [b] The very low efficiency of **R-AN** and **AN** in $^1O_2$ generation.

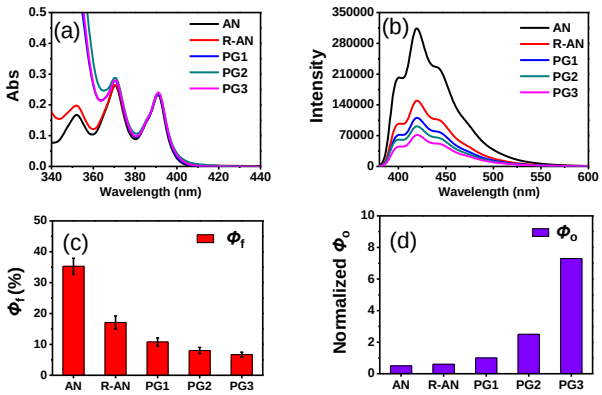

Figure 3. Photosensitization properties of the molecules investigated in this work. UV-vis spectra (a), PL spectra (b), fluorescence quantum yield (c) and $^1O_2$ quantum yield (d) of the resultant rotaxane-branched dendrimers **PG1–PG3**, the precursor [2]rotaxane **R-AN** and the monomer **AN**.

To investigate the mechanism of the enhanced photosensitization efficiencies of these rotaxane-branched dendrimers, time-dependent density functional theory (TD-DFT) calculations were performed on these optimized molecular models **AN**, **R-ANM** and **PG1** in both singlet and triplet excited states (see computational details in the Section E of the SI).[17] According to the perturbation theory-based equation, both the energy gap between the singlet and triplet states (ΔE_{ST}) and SOC should be taken into consideration in studying the ISC since a reduction in ΔE_{ST} or increase in SOC increases the rate constant of ISC (k_{ISC}). As shown in Figure 4 and Table S4-5, **AN**, **R-ANM** and **PG1** exhibited nearly the same ΔE_{ST} because the π-conjugation length of the anthracene moieties in these compounds was the same. Since the **AN** molecule possesses two anthryl units, the S_1 and S_2 states should be nearly degenerated, that is similar to T_1 and T_2 states. Thus, the energy of the upper

excited states (T_n and S_n) did not move closer to the lowest excited states (T_1/T_2 and S_1/S_2). Analysis of the transition configurations of excited states and the corresponding molecular orbitals for **AN**, **R-ANM** and **PG1** confirmed the significant localized excitation (LE) character on anthracene moieties (Figures S37, S38 and S41). This was also in good agreement with the measured absorption and fluorescence spectra. Although the introduction of multiple anthracene units into the rotaxane-branched dendrimers did not induce a decrease in ΔE_{ST}, it is noteworthy that the increased number of anthracene units with the increasing dendrimer generation resulted in the significantly enhanced energy transition channels from S_1/S_2 to T_1/T_2, which was highly beneficial for the ISC process to facilitate $^1O_2$ generation. For instance, unlike **AN** and **R-ANM**, which each possess only one transition channel from S_1/S_2 to T_1/T_2, three times the transition channels from S_1/S_2 to T_1/T_2 occurred in **PG1**, thus endowing **PG1** with a higher photosensitization capability than **AN** and **R-ANM**. Therefore, when the number of anthracene units are further increased in **PG2** and **PG3**, the energy transition channels for ISC from S_1/S_2 to T_1/T_2 should increase accordingly. As a result, the $^1O_2$ generation efficiencies of **PG2** and **PG3** were higher than those **AN**, **R-ANM**, and **PG1**.

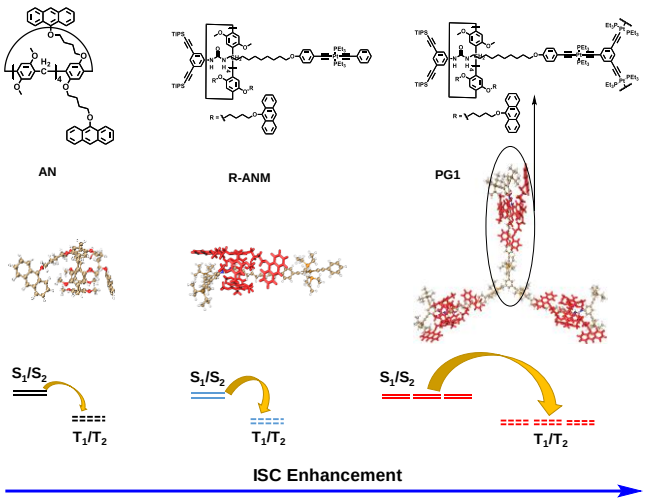

Figure 4. Mechanism of the enhanced photosensitization efficiencies of rotaxane-branched dendrimers. Optimized ground-state geometries of model compounds (top) and calculated excited-state energy levels and possible ISC channels (bottom).

Subsequently, the heavy-atom effect of platinum, which makes an important contribution to SOC, was also studied for **AN**, **R-ANM**, and **PG1**. For **AN**, the significant ISC processes between S_1/S_2 and T_3/T_4 are competitive due to the simultaneous small energy gaps ΔE_{ST} (0.220 ~ 0.247 eV) and moderate SOC values (0.014 ~ 0.223 cm^{-1}) compared to those between S_1/S_2 and T_1/T_2 (ΔE_{ST} of 1.890~1.920 eV and SOC of 0.014~0.099 cm^{-1}) as shown in Table S4. The calculated SOC values of **AN** between S_1/S_2 and T_1/T_2 were relatively small, which is a common phenomenon observed in pure organic compounds. However, for **R-ANM**, upon incorporation of platinum(II) atom from one side, the ISC channels are significantly enhanced between S_1/S_2 and T_1/T_2 (ΔE_{ST} of 1.836~1.906 eV and SOC of 0.022~0.298 cm^{-1}), but the channels between S_1/S_2 and T_3/T_4 states are greatly suppressed due to the vanishing SOC values of 0.000~0.033 cm^{-1}. Furthermore, three times the number of ISC channels for **PG1M** occur accompanying with enhanced SOC values between S_1/S_2 and T_1/T_2 states (see Table S5). Moreover, the T_1/T_2 energy levels (1.65 ~ 1.69 eV) of all the molecules are found to be close to the excitation energy (1.627 eV) for the excited singlet $^1O_2$,[17c] indicating the photosensitization efficiency of $^1O_2$ should be efficient due to the energy-level matching principle. Collectively, the simple introduction of multiple anthracene moieties and platinum atoms on the axles and wheels of the rotaxane units, which resulted in the enhanced energy transition channels from S_1/S_2 to T_1/T_2 and the intramolecular-space heavy-atom effect, respectively, played important roles in improving both the ISC efficiency as well as the $^1O_2$ generation efficiency. Moreover, because of the existence of many more ISC processes from singlet to triplet states, the corresponding nonradiative transition processes became increasingly competitive. Thus the fluorescence quantum yield was gradually reduced from **AN** to **R-ANM** and then to **PG1**–**PG3**.

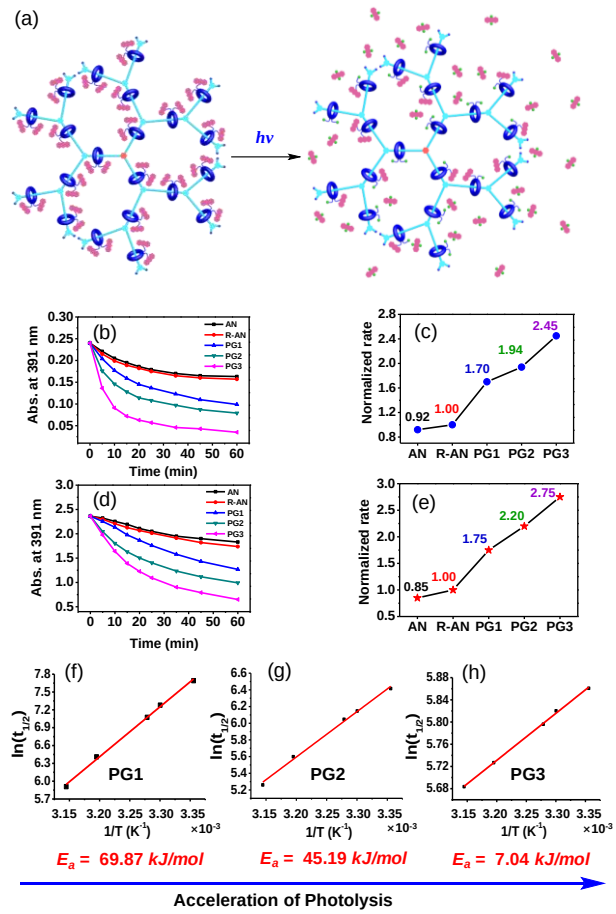

Figure 5. Photolysis of the resultant rotaxane-branched dendrimers **PG1**–**PG3**, the precursor [2]rotaxane **R-AN** and the monomer **AN**. (a) Schematic representation of photolysis of the rotaxane-branched dendrimer **PG3**. Absorbance at 391 nm (b) and normalized photolysis rates (c) upon irradiation at 365 nm for 1 h (0.042 mM, 25 °C). Absorbance at 391 nm (d) and normalized photolysis rates (e) upon irradiation at 365 nm for 1 h (0.42 mM, 25 °C). (f-h) Kinetic analysis of the photolysis of the rotaxane-branched dendrimer **PGn** (n = 1, 2, 3).

Model Photolysis Reactions for Further Investitaion on the Enhanced Photosensitization. It has been reported

that 9-alkoxy-substituted anthracene has the ability to trap $^1O_2$ and then react with it to decompose anthracene into anthraquinone and alkanol through photolysis reaction, which is useful for the detection of $^1O_2$ by directly monitoring the absorption of 9-alkoxy-substituted anthracene.[18] Thus, to further verify the enhanced photosensitization efficiencies of rotaxane-branched dendrimers with the increase of dendrimer generation, the photolysis of the monomer **AN**, the precursor [2]rotaxane **R-AN**, and the resultant rotaxane-branched dendrimers **PG1–PG3** was investigated. As shown in Figure 5a-e, upon irradiation of **AN** (0.042 mM of anthracene unit) at 365 nm for 60 min, the absorption of the 9-alkoxy-substituted anthracene moiety in the range of 340-410 nm gradually decreased. Comparatively, under the same conditions, the irradiation of rotaxane-branched dendrimer **PG1** induced a significant decrease in the absorption of the 9-alkoxy-substituted anthracene moiety with a 2-fold normalized photodecomposition rate higher than that of **AN** (0.92 for **AN**). Along with the increase of the generation of rotaxane-branched dendrimers, the normalized photodecomposition rates for **R-AN**, **PG1**, **PG2**, and **PG3** increased from 1.00, to 1.70, 1.94, and then to 2.45. Moreover, the concentration of the dendrimers had a slight impact on the photodecomposition process. For instance, at higher anthracene unit concentrations (0.42 mM), the normalized photodecomposition rates for **AN**, **R-AN**, **PG1**, **PG2**, and **PG3** were determined to be 0.85, 1.00, 1.75, 2.20, and 2.75, respectively. These results clearly indicated that the formation of rotaxane was beneficial to the photolysis of anthracene, which was significantly enhanced after the formation of the rotaxane-branched dendrimers.

To probe their photolysis mechanism, the photolytic products of **AN**, **R-AN**, **PG1**, and **PG2** were identified by ESI-MS and ^{1}H NMR techniques. For example, upon irradiation with **AN** for 60 min, the precipitate product was separated through filtration and confirmed as anthraquinone by ESI-MS and ^{1}H NMR measurements as shown in Figures S55-56. Moreover, the peak corresponding to the alkanol-substituted pillararene moiety was also observed in the ESI-MS spectrum (Figure S57). These results revealed that **AN** was decomposed into anthraquinone and alkanol-substituted pillararene through photolysis reactions, which was consistent with the reported mechanism.[18b] In the cases of **R-AN**, **PG1**, and **PG2**, the anthraquinone product was also identified by ESI-MS and ^{1}H NMR measurements. Furthermore, ^{1}H NMR analysis demonstrated that the main skeletons of the resultant rotaxane-branched dendrimers remained intact upon UV irradiation although a residue of unreacted 9-alkoxy-substituted anthracene at the periphery of the dendrimers resulted in the generation of asymmetric dendrimers with some broadened signal peaks (Figures S58-63). By combining all the aforementioned results, a plausible photolysis mechanism for rotaxane-branched dendrimers **PG1–PG3** was deduced as illustrated in Scheme S6, where the 9-alkoxy-substituted anthracene at the periphery of the dendrimers reacted with $^1O_2$ to decompose into anthraquinone and the main skeletons of the resultant rotaxane-branched dendrimers remained after irradiation.

With the aim of exploring the mechanism behind the accelerated photolysis reaction of the rotaxane-branched dendrimers, the apparent activation energy (E_a) of **PG1–PG3** was investigated since the E_a of chemical reactions plays a central role in the field of chemical kinetics and serves as an important tool for analyzing and understanding reaction rates.[19] According to the Arrhenius analysis, E_a can be calculated based on the following equation:

$$ln(\mathrm{t}_{1/2}) = \frac{Ea}{R} \times \frac{1}{T} + lnC + lnA$$

where the half-life ($t_{1/2}$), which is highly dependent on temperature, can be obtained directly from the time-conversion curves. A, R, and T are the pre-exponential factor, universal gas constant and temperature, respectively. Therefore, from the data on half-life ($t_{1/2}$) at different temperatures (T), the E_a values for **PG1** and **PG2** were calculated to be 69.87 kJ mol^{-1} and 45.19 kJ mol^{-1}, whereas the E_a value for **PG3** was determined to be only 7.04 kJ mol^{-1} (Figure 5f-h). This result clearly exhibited that increasing generations of the resultant rotaxane-branched dendrimers greatly decreased the apparent activation energy by 62.83 kJ mol^{-1}, which might account for the significant acceleration of the photolysis reaction.

CONCLUSION

In summary, we have developed a novel platform of the rotaxane-branched dendrimers for the construction of highly effective photosensitizers. A series of new rotaxane-branched dendrimers **PG1–PG3** containing up to twenty-one heavy atoms and forty-two photosensitizer moieties were prepared through an efficient and controllable divergent approach. Impressively, the first-, second-, and third-generation rotaxane-branched dendrimers **PG1**, **PG2**, and **PG3** revealed 1.8-, 4.5-, and 13.3-fold higher $^1O_2$ generation efficiency than their corresponding monomer **AN**. The achievement of highly efficient $^1O_2$ generation efficiencies of **PG1-PG3** was atributed to the simple and effective introduction of numerous anthracene moieties and multiple heavy atoms on the axles and wheels of the rotaxane units. These star-shaped, highly topologically branched, and mechanically interlocked rotaxane-branched dendrimers are a very promising platform not only for the preparation of effective photosensitizers but also for the fabrication of artificial light-harvesting systems, photolyzable materials, and dynamic smart materials in the future.

ASSOCIATED CONTENT

Supporting Information. The Supporting Information is available free of charge on the ACS Publications website.
Additional information concerning the synthesis, characterization, and other experimental details.

AUTHOR INFORMATION

Corresponding Author

* hbyang@chem.ecnu.edu.cn (H.-B. Yang)
* lxu@chem.ecnu.edu.cn (L. Xu)

* htsun@phy.ecnu.edu.cn (H. Sun)

ORCID

Hai-Bo Yang: 0000-0003-4926-1618

Notes

The authors declare no competing interest.

ACKNOWLEDGMENT

This work was financially supported by the NSFC/China (Nos. 21922506, 21871092, 21625202, 51773073, 11727810, and 21603074), Shanghai Pujiang Program (No. 18PJD015), the Innovation Program of Shanghai Municipal Education Commission (no. 2019-01-07-00-05-E00012), Projects from Shanghai Science and Technology Commission (No. 19JC1412200), and the Fundamental Research Funds for the Central Universities.

REFERENCES

(1) (a) Bruns, C. J.; Stoddart, J. F. *The Nature of the Mechanical Bond* (John Wiley & Sons, Hoboken, **2016**). (b) Meng, Z.; Xiang, J.-F.; Chen, C.-F. Directional molecular transportation based on a catalytic stopper-leaving rotaxane system. *J. Am. Chem. Soc.* **2016**, *138*, 5652- 5658. (c) Goujon, A.; Du, G.; Moulin, E.;Fuks, G.; Maaloum, M.; Buhler, E.; Giuseppone, N. Hierarchical self-assembly of supramolecular muscle-like fibers. *Angew. Chem. Int. Ed.* **2016**, *55*, 703-707. (d) Erbas-Cakmak, S.; Leigh, D. A.; McTernan, C. T.; Nussbaumer, A. L. Artificial molecular machines. *Chem. Rev.* **2015**, *115*, 10081-10206. (e) Mena-Hernando, S.; Pérez, E. M. Mechanically interlocked materials. Rotaxanes and catenanes beyond the small molecule. *Chem. Soc. Rev.* **2019**, *48*, 5016-5032. (f) Inthasot, A.; Tung, S.-T.; Chiu, S.-H. Using alkali metal ions to template the synthesis of interlocked molecules. *Acc. Chem. Res.* **2018**, *51*, 1324-1337.

(2) (a) Cheng, C.; McGonigal, P. R.; Schneebeli, S. T.; Li, H.; Vermeulen, N. A.; Ke, C.; Stoddart, J. F. An artificial molecular pump. *Nat. Nanotechnol.* **2015**, *10*, 547-553. (b) Qiu, Y.; Zhang, L.; Pezzato, C.; Feng, Y.; Li, W.; Nguyen, M. T.; Chen, C.; Shen, D.; Guo, Q.-H.; Shi, Y.; Cai, K.; Alsubaie, F. M.; Astumian, R. D.; Stoddart, J. F. A molecular dual pump. *J. Am. Chem. Soc.* **2019**, *141*, 17472-17476.

(3) (a) Badjic, J. D.; Balzani, V.; Credi, A.; Stoddart, J. F. A molecular elevator. *Science* **2004**, *303*, 1845-1849. (b) Zhang, Z.-J.; Han, M.; Zhang, H.-Y.; Liu Y. A double-leg donor–acceptor molecular elevator: new insight into controlling the distance of two platforms. *Org. Lett.* **2013**, *15*, 1698–1701.

(4) (a) Anelli, P. L.; Spencer, N.; Stoddart, J. F. A molecular shuttle. *J. Am. Chem. Soc.* **1991**. *113*, 5131-5133. (b) Zhu, K.; Baggi, G.; Loeb, S. J. Ring-through-ring molecular shuttling in a saturated [3]rotaxane. *Nat. Chem.* **2018**, *10*, 625-630. (c) Chen, S.; Wang, Y.; Nie, T.; Bao, C.; Wang, C.; Xu, T.; Lin, Q.; Qu, D.-H.; Gong, X.; Yang, Y.; Zhu, L.; Tian, H. An artificial molecular shuttle operates in lipid bilayers for ion transport. *J. Am. Chem. Soc.* **2018**, *140*, 17992-17998.

(5) (a) Lim, J. Y. C.; Marques, I.; Félix, V.; Beer, P. D. A chiral halogen-bonding [3]rotaxane for the recognition and sensing of biologically relevant dicarboxylate anions. *Angew. Chem. Int. Ed.* **2018**, *57*,584–588. (b) Gong, H.-Y.; Rambo, B. M.; Karnas, E.; Lynch, V. M.; Sessler, J. L. A 'Texas-sized' molecular box that forms an anion-induced supramolecular necklace. *Nat. Chem.* **2010**, *2*, 406–409. (c) Collin, J.-P.; Dietrich-Buchecker, C.; Gaviña, P.; Jimenez-Molero, M. C.; Sauvage, J.-P. Shuttles and muscles: linear molecular machines based on transition metals. *Acc. Chem. Res.* **2001**, *34*, 477-487.(d) Cai, K.; Shi, Y.; Zhuang, G.-W.; Zhang, L.; Qiu, Y.; Shen, D.; Chen, H.; Jiao, Y.; Wu, H.; Cheng, C.; Stoddart, J. F. Molecular-pump-enabled synthesis of a daisy chain polymer. *J. Am. Chem. Soc.* **2020**, *142*, 10308–10313. (e) Cirulli, M.; Kaur, A.; Lewis, J. E. M.; Zhang, Z.; Kitchen, J. A.; Goldup, S. M.; Roessler, M. M. Rotaxane-based transition metal complexes: effect of the mechanical bond on structure and electronic properties. *J. Am. Chem. Soc.* **2019**, *141*, 879-889. (f) Denis, M.; Goldup, S. M. A [3]Rotaxane host selects between stereoisomers. *Angew. Chem. Int. Ed.* **2018**, *57*, 4462-4464. (g) Ogoshi, T.; Aoki, T.; Shiga, R.; Iizuka, R.; Ueda, S.; Demachi, K.; Yamafuji, D.; Kayama, H.; Yamagishi, T.-a. Cyclic host liquids for facile and high-yield synthesis of [2]rotaxanes. *J. Am. Chem. Soc.* **2012**, *134*, 20322-20325. (h) Mitra, R.; Zhu, H.; Grimme, S.; Niemeyer, J. Functional mechanically interlocked molecules: Asymmetric organocatalysis with a catenated bifunctional brønsted acid. *Angew. Chem. Int. Ed*. **2017**, *56*, 11456-11459. (i) Hardie, M. J. One-pot pentaknot. *Nat. Chem*. **2012**, *4*, 7-8. (j) Nakatani, Y.; Furusho, Y.; Yashima, E. Amidinium carboxylate salt bridges as a recognition motif for mechanically interlocked molecules: Synthesis of an optically active [2]catenane and control of its structure. *Angew. Chem. Int. Ed*. **2010**, *49*, 5463-5467. (k) Kim, D. H.; Singh, N.; Oh, J.; Kim, E.-H.; Jung, J.; Kim, H.; Chi, K.-W. Coordination-driven self-assembly of a molecular knot comprising sixteen crossings. *Angew. Chem. Int. Ed.* **2018**, *57*, 5669-5673. (l) Kim, T.; Singh, N.; Oh, J.; Kim, E.-H.; Jung, J.; Kim, H.; Chi, K.-W. Selective synthesis of molecular borromean rings: Engineering of supramolecular topology via coordination-driven self-assembly. *J. Am. Chem. Soc.* **2016**, *138*, 8368-8371. (m) Goujon, A.; Lang, T.; Mariani, G.; Moulin, E.; Fuks, G.; Raya, J.; Buhler, E.; Giuseppone, N. Bistable [c2] Daisy Chain Rotaxanes as Reversible Muscle-like Actuators in Mechanically Active Gels. *J. Am. Chem. Soc.* **2017**, *139*, 14825-14828.

(6) (a) Mao, M.; Zhang, X.-K.; Xu, T.-Y.; Wang, X.-D.; Rao, S.-J.; Liu, Y.; Qu, D.-H.; Tian, H. Towards a hexa-branched [7]rotaxane from a [3]rotaxane via a [2+2+2] alkyne cyclotrimerization Process. *Chem. Commun.* **2019**, *55*, 3525-3528. (b) Kwan, C.-S.; Zhao, R.; Hove, M. A. V.; Cai, Z.; Leung, K. C.-F. Higher-generation type III-B rotaxane dendrimers with controlling particle size in three-dimensional molecular switching. *Nat. Commun*. **2018**, *9*, 497. (c) Lee, J. W.; Han, S. C.; Kim, J. H.; Ko, Y. H.; Kim, K. Formation of rotaxane dendrimers by supramolecular click chemistry. *Bull. Korean Chem. Soc.* **2007**, *28*, 1837-1840. (d) Amabilino, D. B.; Ashton, P. R.; Balzani, V.; Brown, C. L.; Credi, A.; Fréchet, J. M. J.; Leon, J. W.; Raymo, F. M.; Spencer, N.; Stoddart, J. F.; Venturi. M. Self-assembly of [n]rotaxanes bearing dendritic stoppers. *J. Am. Chem. Soc.* **1996**, *118*, 12012-12020. (e) Leung, K. C.-F.; Lau, K. N. Self-assembly and thermodynamic synthesis of rotaxane dendrimers and related structures. *Poly. Chem.* **2010**, *1*, 988-1000. (f) Chen, C.-F. High-generation organometallic rotaxane dendrimer. *Sci. China Chem.* **2015**, *58*, 1089. (g) Kim, S.-Y.; Ko, Y. H.; Lee, J. W.; Sakamoto, S.; Yamaguchi, K.; Kim, K. Toward high-generation rotaxane dendrimers that incorporate a ring component on every branch: noncovalent synthesis of a dendritic [10]pseudorotaxane with 13 molecular components. *Chem. -Asian J.* **2007**, *2*, 747-754.

(7) (a) Ho, W. K.-W.; Lee, S.-F.; Wong, C.-H.; Zhu, X.-M.; Kwan, C.-S.; Chak, C.-P.; Mendes, P. M.; Cheng, C. H. K.; Leung, K. C.-F. Type III-B rotaxane dendrimers. *Chem. Commun*. **2013**, *49*, 10781-10783. (b) Elizarov, A. M.; Chiu, S.-H.; Glink, P. T.; Stoddart, J. F. Dendrimer with rotaxane-like mechanical branching. *Org. Lett.* **2002**, *4*, 679-682. (c) Zeng, Y.; Li, Y.; Li, M.; Yang, G.; Li, Y. Enhancement of energy utilization in light harvesting dendrimers by the pseudorotaxane formation at periphery. *J. Am. Chem. Soc.* **2009**, *131*, 9100-9106. (d) Tramontozzi, D. A.; Suhan, N. D.; Eichhorn, S. H.; Loeb, S. J. The effect of incorporating fréchet dendrons into rotaxanes and molecular shuttles containing the 1, 2-bis(pyridinium)ethane⊂[24]crown-8 templating motif. *Chem. Eur. J.* **2010**, *16*, 4466-4476. (e) Lee, J. W.; Kim, K. Rotaxane dendrimers. *Top Curr. Chem.* **2003**, *228*, 111-140. (f) Zhou, H.-Y.; Zong, Q.; Han Y.; Chen, C.-F. Recent advances in higher order rotaxane architectures. *Chem. Commun.* **2020**, 56, 9916-9936.

(8) Wang, X.-Q.; Li, W.-J.; Wang, W.; Wen, J.; Zhang, Y.; Tan, H.; Yang, H.-B. Construction of type III-C rotaxane-branched dendrimers and their anion-induced dimension modulation feature. *J. Am. Chem. Soc.* **2019**, *141*, 13923-13930.

(9) (a) Li, W.-J.; Wang, W.; Wang, X.-Q.; Li, M.; Ke, Y.; Yao, R.; Wen, J.; Yin, G.-Q.; Jiang, B.; Li, X.; Yin, P.; Yang, H.-B. Daisy chain dendrimers: integrated mechanically interlocked molecules with stimuli-induced dimension modulation feature. *J. Am. Chem. Soc.* **2020**, *142*, 8473-8482. (b) Wang, X.-Q.; Wang, W.; Li, W.-J.; Chen, L.-J.; Yao, R.; Yin, G.-Q.; Wang, Y.-X.; Zhang, Y.; Huang, J.; Tan, H.; Yu, Y.; Li, X.; Xu, L.; Yang, H.-B. Dual stimuli-responsive rotaxane-branched dendrimers with reversible dimension modulation. *Nat. Commun.* **2018**, *9*, 3190.

(10) (a) Zhao, J.; Wu, W.; Sun, J.; Guo, S. Triplet photosensitizers: from molecular design to applications. *Chem. Soc. Rev.* **2013**, *42*, 5323-5351. (b) Howlader, P.; Mondal, B.; Purba, P. C.; Zangrando, E.; Mukherjee, P. S. Self-assembled Pd(II) barrels as containers for transient merocyanine form and reverse thermochromism of spiropyran. *J. Am. Chem. Soc.* **2018**, *140*, 7952-7960. (c) Acharyya, K.; Bhattacharyya, S.; Sepehrpour, H.; Chakraborty, S.; Lu, S.; Shi, B.; Li, X.; Mukherjee, P. S.; Stang, P. J. Self-assembled fluorescent Pt(II) metallacycles as artificial light-harvesting systems. *J. Am. Chem. Soc.* **2019,** *141*, 4565–14569. (d) Hola, E.; Ortyl, J.; Jankowska, M.; Pilch, M.; Galek, M.; Morlet-Savary, F.; Graff, B.; Dietlinc, C.; Lalevée, J. New bimolecular photoinitiating systems based on terphenyl derivatives as highly efficient photosensitizers for 3D printing application. *Polym. Chem.* **2020**,*11*, 922-935. (e) Shao, L.; Pan, Y.; Hua, B.; Xu, S.; Yu, G.; Wang, M.; Liu, B.; Huang, F. Constructing adaptive photosensitizers via supramolecular modification based on pillararene host–guest interactions. *Angew. Chem. Int. Ed.* **2020**, *59*, 11779-11783. (f) Li, D.-H.; Schreiber, C. L.; Smith, B. D. Sterically shielded heptamethine cyanine dyes for bioconjugation and high performance near-infrared fluorescence imaging. *Angew. Chem. Int. Ed.* **2020**, *59*, 12154–12161. (g) Wu, W.; Mao, D.; Xu, S.; Kenry, F.; Hu, Li, X.; Kong, D.; Liu, B. Polymerization-enhanced photosensitization. *Chem* **2018**, *4*, 1937-1951. (h) Liu, S.; Zhang, H.; Li, Y.; Liu, J.; Du, L.; Chen, M.; Kwok, R. T. K.; Lam, J. W. Y.; Phillips, D. L.; Tang, B. Z. Strategies to enhance the photosensitization: polymerization and the donor–acceptor even–odd effect. *Angew. Chem. Int. Ed.* **2018**, *57*, 15189-15193. (i) Peck, E. M.; Collins, C. G.; Smith, B. D. Thiosquaraine rotaxanes: synthesis, dynamic structure, and oxygen photosensitization. *Org. Lett.* **2013**, *15*, 2762–2765.

(11) (a) Schmidt, K.; Brovelli, S.; Coropceanu, V.; Beljonne, D.; Cornil, J.; Bazzini, C.; Caronna, T.; Tubino, R.; Meinardi, F.; Shuai, Z.; Brédas, J.-L. Intersystem crossing processes in nonplanar aromatic heterocyclic molecules. *J. Phys. Chem. A* **2007**, *111*, 10490-10499. (b) Espinoza, C.; Trigos, Á.; Medina, M. E. Theoretical study on the photosensitizer mechanism of phenalenone in aqueous and lipid media. *J. Phys. Chem. A* **2016**, *120*, 6103-6110. (c) Jin, J.; Zhu, Y.; Zhang, Z.; Zhang, W. Enhancing the efficacy of photodynamic therapy through a porphyrin/POSS alternating copolymer. *Angew. Chem. Int. Ed.* **2018**, *57*, 16354-16358. (d) Wang, Z.; Zhao, J.; Barbon, A.; Toffoletti, A.; Liu, Y.; An, Y.; Xu, L.; Karatay, A.; Yaglioglu, H. G.; Yildiz, E. A.; Hayvali, M. Radical-enhanced intersystem crossing in new bodipy derivatives and application for efficient triplet–triplet annihilation upconversion. *J. Am. Chem. Soc.* **2017**, *139*, 7831-7842.

(12) (a) Hou, Y.; Liu, Q.; Zhao, J. An exceptionally long-lived triplet state of red light-absorbing compact phenothiazine-styrylBodipy electron donor/acceptor dyads: a better alternative to the heavy atom-effect? *Chem. Commun.* **2020**, *56*, 1721-1724. (b) Yu, Q.; Huang, T.; Liu, C.; Zhao, M.; Xie, M.; Li, G.; Liu, S.; Huang, W.; Zhao, Q. Oxygen self-sufficient NIR-activatable liposomes for tumor hypoxia regulation and photodynamic therapy. *Chem. Sci.* **2019**, *10*, 9091-9098. (c) Karges, J.; Basu, U.; Blacque, O.; Chao, H.; Gasser, G. Polymeric encapsulation of novel homoleptic bis(dipyrrinato) zinc(II) complexes with long lifetimes for applications as photodynamic therapy photosensitisers. *Angew. Chem. Int. Ed.* **2019**, *58*, 14334-14340. (d) Gorman, A.; Killoran, J.; O'Shea, C.; Kenna, T.; Gallagher, W. M.; O'Shea, D. F. In vitro demonstration of the heavy-atom effect for photodynamic therapy. *J. Am. Chem. Soc.* **2004**, *126*, 10619-10631.

(13) Wang, W.; Chen, L.-J.; Wang, X.-Q.; Sun, B.; Li, X.; Zhang, Y.; Shi, J.; Yu, Y.; Zhang, L.; Liu, M.; Yang, H.-B. Organometallic rotaxane dendrimers with fourth-generation mechanically interlocked branches. *Proc. Natl. Acad. Sci. U. S. A.* **2015**, *112*, 5597-5601.

(14) (a) Fan, C.; Wu, W.; Chruma, J. J.; Zhao, J.; Yang, C. Enhanced triplet–triplet energy transfer and upconversion fluorescence through host–guest complexation. *J. Am. Chem. Soc.* **2016**, *138*, 15405-15412. (b) Cekli, S.; Winkel, R. W.; Alarousu, E.; Mohammed, O. F.; Schanze, K. S. Triplet excited state properties in variable gap π-conjugated donor–acceptor–donor chromophores. *Chem. Sci.* **2016**, *7*, 3621-3631.

(15) (a) Chan, A. K.-W.; Ng, M.; Wong, Y.-C.; Chan, M.-Y.; Wong, W.-T.; Yam, V. W.-W. Synthesis and characterization of luminescent cyclometalated platinum(II) complexes with tunable emissive colors and studies of their application in organic memories and organic light-emitting devices. *J. Am. Chem. Soc.* **2017**, *139*, 10750-10761. (b) Wang, X.; Han, Y.; Liu, Y.; Zou, G.; Gao, Z.; Wang, F. Cooperative supramolecular polymerization of fluorescent platinum acetylides for optical waveguide applications. *Angew. Chem. Int. Ed.* **2017**, *56*, 12466-12470. (c) Furusho, Y.; Tanaka, Y.; Yashima, E. Double helix-to-double helix transformation, using platinum(II) acetylide complexes as surrogate linkers, *Org. Lett.* **2017**, *8*, 2583–2586. (d) Ito, H.; Ikeda, M.; Hasegawa, T.; Furusho, Y.; Yashima, E. Synthesis of complementary double-stranded helical oligomers through chiral and achiral amidinium-carboxylate salt bridges and chiral amplification in their double-helix formation, *J. Am. Chem. Soc.* **2011**, *133*, 3419–3432. (e) Leininger, S.; Stang, P. J.; Huang, S. Synthesis and characterization of organoplatinum dendrimers with 1, 3, 5-triethynylbenzene building blocks. *Organometallics* **1998**, *17*, 3981-3987. (f) Wang, W.; Yang, H.-B.; Linear neutral platinum–acetylide moiety: beyond the links. *Chem. Commun.* **2014**, *50*, 5171-5186.

(16) (a) Kim, S.; Fujitsuka, M.; Majima, T. Photochemistry of singlet oxygen sensor green. *J. Phys. Chem. B* **2013**, *117*, 13985–13992. (b) Prasad, A.; Sedlářová, M.; Pospíšil, P. Singlet oxygen imaging using fluorescent probe singlet oxygen sensor green in photosynthetic organisms. *Sci. Rep.* **2018**, *8*, 13685. (c) Yu, G.; Zhu, B.; Shao, L.; Zhou, J.; Saha, M. L.; Shi, B.; Zhang, Z.; Hong, T.; Li, S.; Chen, X.; Stang, P. J. Host–guest complexation-mediated codelivery of anticancer drug and photosensitizer for cancer photochemotherapy. *Proc. Natl. Acad. Sci. U.S.A.*, **2019**, *116*, 6618-6623. (d) Zhao, Y.; Farrer, N. J.; Li, H.; Butler, J. S.; McQuitty, R. J.; Habtemariam, A.; Wang, F.; Sadler, P. J. De novo generation of singlet oxygen and ammine ligands by photoactivation of a platinum anticancer complex. *Angew. Chem. Int. Ed.*, **2013**, *52*, 13633-13637. (e) Chen, Y.-Z.; Wang, Z. U.; Wang, H.; Lu, J.; Yu, S.-H.; Jiang, H.-L. Singlet oxygen-engaged selective photo-oxidation over Pt nanocrystals/porphyrinic MOF: the roles of photothermal effect and Pt electronic state. *J. Am. Chem. Soc.*, **2017**, *139*, 2035-2044. (f) Chen, L.-J.; Chen, S.; Qin, Y.; Xu, L.; Yin, G.-Q.; Zhu, J.-L.; Zhu, F.-F.; Zheng, W.; Li, X.; Yang, H.-B. Construction of porphyrin-containing metallacycle with improved stability and activity within mesoporous carbon. *J. Am. Chem. Soc.*, **2018**, *140*, 5049-5052. (g) Qin, Y.; Chen, L.-J.; Dong, F.; Jiang, S.-T.; Yin, G.-Q.; Li, X.; Tian, Y.; Yang, H.-B. Light-controlled generation of singlet oxygen within a discrete dual-stage metallacycle for cancer therapy. *J. Am. Chem. Soc.*, **2019**, *141*, 8943-8950.

(17) (a) Marques, M. A. L.; Ullrich, C. A.; Nogueira, F.; Rubio, A.; Burke, K.; Gross, E. K. U. Time-dependent density functional theory (Springer: Berlin, Germany, **2006**, 706). (b) Runge, E.; Gross, E. K. U. Density-functional theory for time-dependent systems. *Phys. Rev. Lett.* **1984**, *52*, 997–1000. (c) Schweitzer, C.; Schmid, R. Physical mechanisms of generation and deactivation of singlet oxygen. *Chem. Rev.* **2003**, *103*, 1685–1757.

(18) (a) He, Y.-Q.; Fudickar, W.; Tang, J.-H.; Wang, H.; Li, X.; Han, J.; Wang, Z.; Liu, M.; Zhong, Y.-W.; Linker, T.; Stang, P. J. Capture and release of singlet oxygen in coordination-driven self-assembled organoplatinum(II) metallacycles. *J. Am. Chem. Soc.* **2020**, *142*, 2601-2608; (b) Wang, Y.-X.; Zhang, Y.-M.; Liu, Y. Photolysis of an amphiphilic assembly by calixarene-induced aggregation. *J. Am. Chem. Soc.* **2015**, *137*, 4543-4549. (c) Preston, D.; Sutton, J. J.; Gordon, K. C.; Crowley, J. D. A nona-nuclear heterometallic Pd3Pt6 "donut"-shaped cage: molecular recognition and photocatalysis. *Angew.*

Chem. Int. Ed. **2018**, *57*, 8659-8663. (d) Kim, S.; Tachikawa, T.; Fujitsuka, M.; Majima, T. Far-red fluorescence probe for monitoring singlet oxygen during photodynamic therapy. *J. Am. Chem. Soc.* **2014**, *136*, 11707-11715. (e) Yoshizawa, M.; Catti, L. Bent anthracene dimers as versatile building blocks for supramolecular capsules. *Acc. Chem. Res.* **2019**, *52*, 2392–2404. (f) Sekiguchi, S.; Kondo, K.; Sei, Y.; Akita, M.; Yoshizawa, M. Engineering stacks of V-shaped polyaromatic compounds with alkyl chains for enhanced emission in the solid state. *Angew. Chem. Int. Ed.* **2016**, *55*, 6906 –6910.

(19) (a) Mao, Z.; Campbell, C. T. Apparent activation energies in complex reaction mechanisms: a simple relationship via degrees of rate control. *ACS Catal.* **2019**, *9*, 9465-9473. (b) Jiao, Y.; Li, W.-L.; Xu, J.-F.; Wang, G.; Li, J.; Wang, Z.; Zhang, X. A supramolecularly activated radical cation for accelerated catalytic oxidation. *Angew. Chem. Int. Ed.* **2016**, *55*, 8933-8937.

Insert Table of Contents artwork here